

On statistically stationary homogeneous shear turbulence

Jörg Schumacher and Bruno Eckhardt

Fachbereich Physik, Philipps-Universität Marburg, D-35032 Marburg, Germany

(December 2, 2024)

A statistically stationary turbulence with a mean shear gradient is realized in a flow driven by suitable body forces. The flow domain is periodic in downstream and spanwise directions and bounded by stress free surfaces in the normal direction. Except for small layers near the surfaces the flow is homogeneous. The fluctuations in turbulent energy are less violent than in the simulations using remeshing, but the anisotropy on small scales as measured by the skewness of derivatives is similar.

Introduction.— Although most flows in nature and laboratory are anisotropic on large scales the statistical behaviour on small scales is expected to become isotropic [1,2]. This seems to be supported by experiment and numerical analysis on the level of second order moments [3–5]. However, motivated by analogous behaviour in the passive scalar problem, Pumir and Shraiman suggested that higher order moments might remain anisotropic even for large Reynolds number [6,7]. It would seem that a natural situation in which to investigate this problem is that of a homogeneous shear flow, in which the time averages $\langle \cdot \rangle$ of the velocity field are independent of the position in space and satisfy

$$\langle u_x \rangle = Sy, \quad \langle u_y \rangle = \langle u_z \rangle = 0, \quad (1)$$

with (constant) shear rate S . Despite its simple appearance, both experimental and numerical realizations of this flow are problematic. In the experiment the mean shear is produced by suitable constraints behind a grid, so that the turbulence is advected and decaying and eventually influenced by rigid walls. The incompatibility of stationarity and homogeneity in such flows has been discussed in detail by Corrsin *et al.* [8–10]. In numerical simulations using the pseudospectral technique the mean shear was always implemented by the Rogallo remeshing procedure, which corresponds to a time-periodic driving of the flow [11,7]. Our aim here is to present an alternative numerical approach to simulations of homogeneous shear flows that avoids the periodic driving and allows to maintain a statistically stationary state for long times.

Numerical Implementation.— With length scales measured in units of the gap width d , and time scales in units of S , the dimensionless form of the equations for an incompressible Navier–Stokes fluid become

$$\frac{\partial \mathbf{u}}{\partial t} + (\mathbf{u} \cdot \nabla) \mathbf{u} = -\nabla p + \frac{1}{Re_s} \nabla^2 \mathbf{u} + \mathbf{f}, \quad (2)$$

$$\nabla \cdot \mathbf{u} = 0 \quad (3)$$

where $p(\mathbf{x}, t)$ is the pressure, $\mathbf{u}(\mathbf{x}, t)$ the velocity field. The shear Reynolds number is $Re_s = S d^2 / \nu$ with ν as kinematic viscosity. In the x (streamwise) and z (spanwise) directions periodic boundary conditions apply. In

the other direction the flow domain is bounded by two parallel flat surfaces that are assumed to be impenetrable and stress-free, *i.e.* $u_y = \partial_y u_x = \partial_y u_z = 0$. The effects of the free slip surfaces at $y = 0$ and $y = d$ on the bulk behaviour are much weaker than those of rigid walls, since only the wall-normal component is forced to vanish. The resulting boundary layer in the wall normal component is of the order $\nu / u'_{y, rms}$ where $u'_{y, rms} = \langle (u'_y)^2 \rangle^{1/2}$ denotes the root mean square fluctuations of the turbulent wall normal velocity. The statistical properties of the tangential components are not affected by this boundary layer.

The mean shear and turbulence are maintained by a suitable body force $\mathbf{f}(\mathbf{x}, t)$. An almost linear mean profile $\langle u_x \rangle(y) = S(1/2 - y)$ for $y \in [0, 1]$ (in dimensionless form) can be approximated by a finite Fourier sum of cosines

$$\langle u_x \rangle(y) = \frac{4S}{\pi^2} \sum_{n=0}^5 \frac{\cos[(2n+1)\pi y]}{(2n+1)^2}. \quad (4)$$

The external forcing \mathbf{f} was chosen such that the six modes used in eq. (4) remained constant in time, *i.e.* $\partial_t \text{Re } u_x(\mathbf{q}, t) = 0$ for Fourier modes with $\mathbf{q} = (2n+1)\pi \mathbf{e}_y$ for $n = 0$ to 5. At sufficiently high shear rates the flow is unstable and turbulence sets in. Then the force \mathbf{f} fluctuates in time as well.

The free slip boundary conditions allow for efficient numerical simulations with Fourier modes for the velocity components. Nevertheless, the data presented here amount to approximately 360 CPU hours of computing time on a Cray T-90. The equations are integrated by means of a pseudospectral technique using a 2/3-rule dealiasing. The integration domain has an aspect ratio $L_x : L_y : L_z = 2\pi d : d : 2\pi d$ and is resolved by $256 \times 65 \times 256$ Fourier modes.

Stationarity.— When averaged in downstream and spanwise direction as well as in time, the mean velocity components show the expected shear flow behaviour, $\langle u_y \rangle = \langle u_z \rangle = 0$ and $\langle u_x \rangle \approx -Sy$ (see fig. 1). The downstream profile differs from the linear shear flow only in a small region near the surfaces; this region decreases as the Reynolds number increases (inset of fig. 1). Before starting the statistical analysis a forward integration over a

period of $ST \geq 20$ (time is measured in units of the shear rate S) with the full spectral resolution was always performed to guarantee relaxation to the turbulent state.

The fluctuations in the velocity field are defined as $u'_i = u_i - \langle u_i \rangle$ for $i = x, y, z$. Figure 2 shows the time evolution of the total kinetic energy in the fluctuations, $q^2(t) = \langle (u'_i)^2 \rangle_V$, where $\langle \cdot \rangle_V$ denotes an average over the volume. The amplitude of the variations in kinetic energy decreases with increasing Reynolds number. This seems to be connected to the fragmentation of coherent streaks and vortices [12,13] with increasing Re and the reduced downstream correlation. This is shown by volume surface plots of the turbulent streamwise velocity component at the lowest (see fig. 3) and the highest (see fig. 4) of our Reynolds numbers. The periods of the oscillations in total kinetic energy are surprisingly large, thus requiring very long time integrations for converged time averages. Compared to the long time simulations of Pumir [7] the fluctuations are smaller in amplitude and do not show the violent bursts.

Finally, statistical stationarity implies balancing of the turbulent kinetic energy in the mean,

$$0 = -\nu \langle [\partial_i u'_j (\partial_i u'_j + \partial_j u'_i)] \rangle - \langle u'_x u'_y \rangle \partial_y \langle u_x \rangle + \langle u'_x f'_x \rangle. \quad (5)$$

The first term on the right side is the energy dissipation rate ϵ and the second term is the turbulent energy production rate P . The last term, is the energy injection due to the applied volume forcing. In the bulk, outside the small boundary layers near the top and bottom surfaces, we find that the production and dissipation differ by less than 4% and that the energy injection from the volume forcing is negligibly small. Here we took volume and time averages for the Reynolds stress component in the production term, for the energy dissipation rate and the energy injection term. We used an averaging time in shear rate units, *i.e.* ST , of 75 for the lower R_λ and 50 as well as 100 for the highest R_λ .

Higher order statistical moments.— Data on statistical moments from the experiment of Garg and Warhaft [14], two sets of direct numerical simulations [7] and [15] and our simulations are collected in table I. The data sets cover almost the same range of parameters with similar behaviour, despite the different realizations of the mean shear. The dimensionless $S^* = Sq^2/\epsilon$ does not seem to vary with Re_s , but $S(\nu/\epsilon)^{1/2}$ decreases for our range of Re_s . This agrees with the observations of Pumir and Shraiman [6,7].

	Exp. [14]	DNS [15]	DNS [7]	$Re_s = 500$	$Re_s = 1000$	$Re_s = 2000$
$\langle (u'_x)^2 \rangle / q^2$	—	0.53	0.53	0.57	0.55	0.52 (0.52)
$\langle (u'_y)^2 \rangle / q^2$	—	0.16	0.21	0.12	0.15	0.18 (0.17)
$\langle (u'_z)^2 \rangle / q^2$	—	0.31	0.26	0.31	0.30	0.30 (0.31)
$S_1^* = S \langle (u'_x)^2 \rangle / \epsilon$	3.31	4.58	3.98	4.17	4.72	4.20 (4.26)
$S^* = Sq^2 / \epsilon$	—	8.65	7.50	7.32	8.58	8.08 (8.19)
$S(\nu/\epsilon)^{1/2}$	0.04	—	0.11	0.38	0.25	0.18 (0.17)
P/ϵ	0.96	—	—	1.04	0.99	1.02 (0.98)
R_λ	310	73	90	59	87	94 (106)
S_{ω_z}	—	—	-0.58	-0.79	-0.67	-0.57 (-0.60)
K_{ω_z}	—	—	—	5.62	6.57	7.36 (7.45)
$S_{\partial u'_x / \partial y}$	0.5	—	0.87	0.96	0.90	0.82 (0.84)
$K_{\partial u'_x / \partial y}$	8.6	—	—	5.59	6.38	7.08 (7.14)

TABLE I. Comparison between experiment and different simulations on homogeneous shear turbulence. The Taylor-Reynolds number is calculated from $R_\lambda = \langle (u'_x)^2 \rangle / \nu [(\partial_x u'_x)^2]^{1/2}$. The skewness and kurtosis of a field ϕ are defined as $S_\phi = \langle \phi^3 \rangle / \langle \phi^2 \rangle^{3/2}$ and $K_\phi = \langle \phi^4 \rangle / \langle \phi^2 \rangle^2$, respectively. Note that here the total kinetic energy $q^2 = \langle (u'_i)^2 \rangle$ is also averaged in time. The values given in parentheses in the last column are obtained by averaging over a time interval twice as long.

Most quantities in table I change monotonically with Re_s . We attribute the few exceptions to peculiarities of the simulations at $Re_s = 500$ which has the strongest coherent structures and is perhaps most strongly affected by the downstream periodicity. It is interesting to note that coherent structures (predominantly streaks and downstream vortices) show up in all our simulations, even at the lowest Reynolds number. In the simulations of [16] that used remeshing they were observed for higher

values of S^* only, where their flow became strongly non-stationary. The effects of vortices and downstream periodicity may also explain the rather large skewness values S_{ω_z} and $S_{\partial u'_x / \partial y}$ for $Re_s = 500$. Both quantities decrease steadily with R_λ , while they remained constant ($\sim R_\lambda^0$) in the simulations of Ref. [7]. The shear flow experiments [14] have been fitted to $\sim R_\lambda^{-0.6}$ for $150 \lesssim R_\lambda \lesssim 400$. The data currently available are insufficient to draw conclusions on the asymptotic scaling.

The effects of the surfaces on the higher order moments are limited to the boundary layers very close to the surfaces. The spatially resolved plots in fig. 5 show the shear direction dependence of the skewness and kurtosis of the spanwise vorticity, $\omega_z = \partial_x u'_y - \partial_y u'_x$, and the shear gradient $\partial_y u'_x$. The variations across the shear layer become smaller with increasing Reynolds number.

Summary — The simulations for the statistically stationary shear flows bounded by free slip surfaces show that in the central region an approximately homogeneous shear flow with statistically stationary properties develops. The moments of the velocity field are compatible with previous experimental and numerical findings. The most noticeable difference to the long time simulations by Pumir [7] is the absence of violent bursts in turbulent

energy. Further investigations of the statistical properties of this model for almost homogeneous shear flows are in progress.

Acknowledgments.— We thank L. Biferale, D. Lohse, M. Nelkin, K. Sreenivasan, and F. Toschi for fruitful discussions, A. Pumir for comments on the manuscript, and the Institute for Theoretical Physics at Santa Barbara for hospitality. This work was supported in part by National Science Foundation under Grant No. PHY94-07194 and the European Union within the CARTUM project. The numerical simulations were done on a Cray T-90 at the John von Neumann Institute for Computing at the Forschungszentrum Jülich and we are grateful for their support.

-
- [1] KOLMOGOROV A. N., *Dokl. Akad. Nauk SSSR*, **30** (1941) 301.
 - [2] LUMLEY J. L., *Phys. Fluids*, **10** (1967) 855.
 - [3] SADDUGHI S. and VEERAVALLI S. V., *J. Fluid Mech.*, **268** (1994) 333.
 - [4] FERNHOLZ H. H., KRAUSE E., NOCKERMAN M. and SCHÖBER M., *Phys. Fluids*, **7** (1995) 1275.
 - [5] SHE Z., CHEN S., DOOLEN G., KRAICHNAN R. H. and ORSZAG S., *Phys. Rev. Lett.*, **70** (1993) 3251.
 - [6] PUMIR A. and SHRAIMAN B., *Phys. Rev. Lett.* **75** (1995) 3114.
 - [7] PUMIR A., *Phys. Fluids*, **8** (1996) 3112.
 - [8] CHAMPAGNE F. H., HARRIS V. G. and CORRSIN S., *J. Fluid Mech.*, **41** (1970) 81.
 - [9] HARRIS V. G., GRAHAM J. A. H. and CORRSIN S., *J. Fluid Mech.*, **81** (1977) 657.
 - [10] TAVOULARIS S. and CORRSIN S., *J. Fluid Mech.*, **104** (1981) 311.
 - [11] ROGALLO R. S., *Numerical experiments in homogeneous turbulence*, NASA TM 81315 (1981).
 - [12] SCHUMACHER, J. and ECKHARDT, B., *Evolution of turbulent spots in a plane shear flow*, submitted to Phys. Rev. E (2000).
 - [13] WALEFFE, F., *Phys. Fluids*, **9** (1997) 883.
 - [14] GARG, S. and WARHAFT, Z., *Phys. Fluids*, **10** (1998) 662.
 - [15] ROGERS, M.M. and MOIN, P., *J. Fluid Mech.*, **176** (1987) 33.
 - [16] LEE M. J., KIM J. and MOIN, P., *J. Fluid Mech.*, **216** (1990) 561.

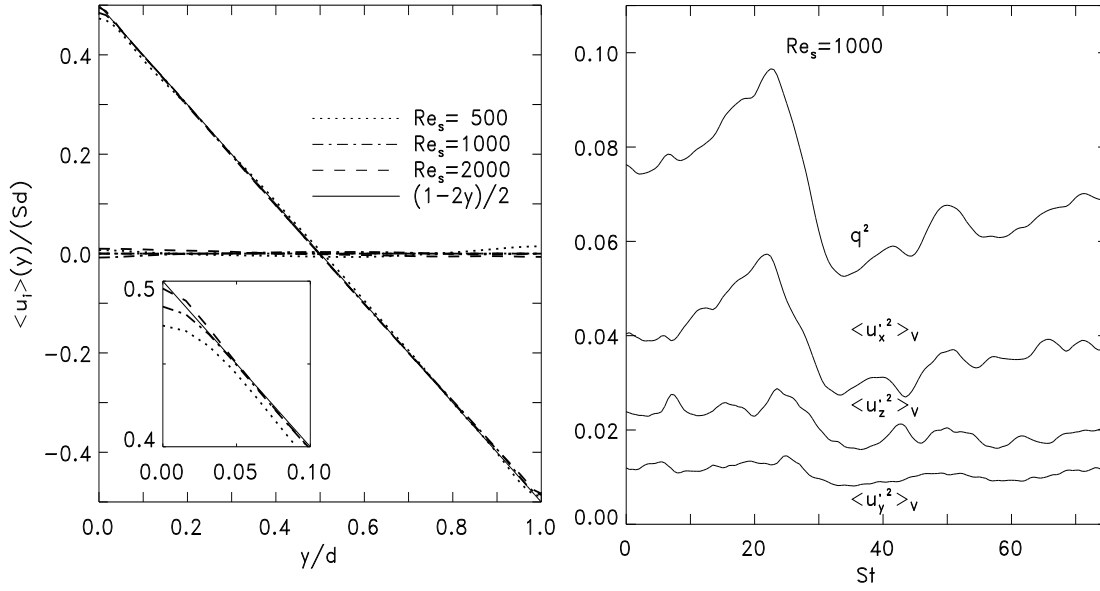


FIG. 1. The mean velocity field $\langle u_i \rangle(y)$, averaged in time and over planes normal to the mean shear, for $Re_s = 500, 1000$ and 2000 . The solid line is the idealized linear function in dimensionless form. The inset resolves the small layer near the surface where the mean shear is not constant.

FIG. 2. Time traces of the turbulent kinetic energy $q^2(t)/(Sd)^2$ and of the separate contributions from the turbulent velocity components $\langle (u_i')^2 \rangle_V / (Sd)^2$ for the three components $i = x, y$ and z .

FIG. 3. (Separate JPG File) Isosurfaces of the streamwise turbulent velocity component u_y' for $Re_s = 500$ at the levels $u_y'/(Sd) = \pm 0.48$. Positive values are darker, negative values brighter.

FIG. 4. (Separate JPG File) Same as fig. 3, but for $Re_s = 2000$ with levels $u_y'/(Sd) = \pm 0.46$. At this higher Reynolds number the flow structures are more fragmented and smaller.

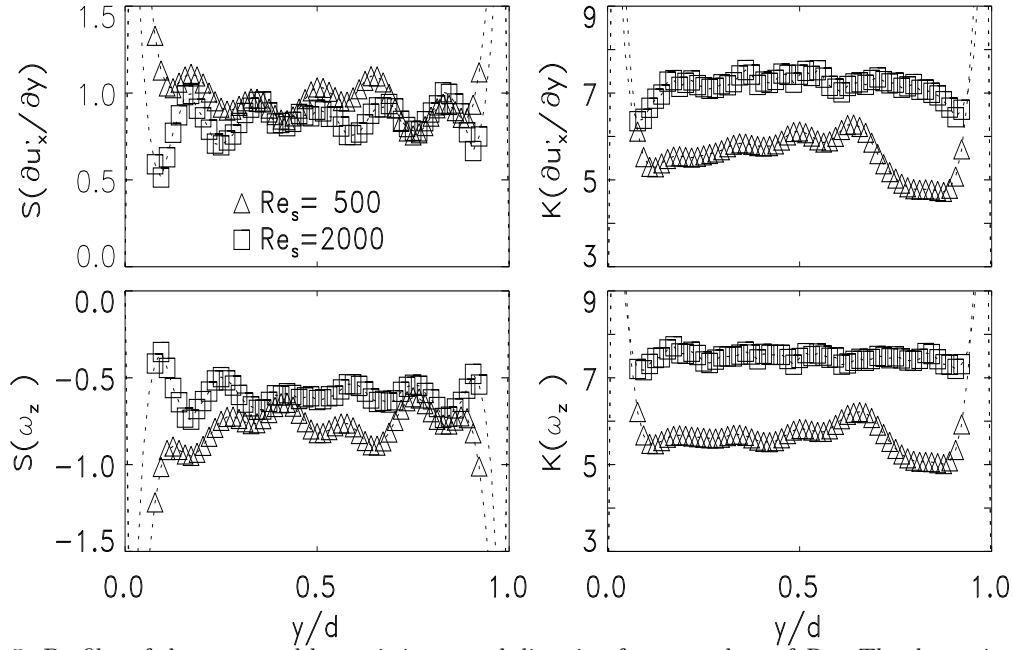


FIG. 5. Profiles of skewness and kurtosis in normal direction for two values of Re_s . The datapoints closest to the boundary surfaces (indicated by dotted lines) are excluded from the statistical analysis that leads to the entry in table. I.

This figure "Figure3.jpg" is available in "jpg" format from:

<http://arxiv.org/ps/nlin/0005021v2>

This figure "Figure4.jpg" is available in "jpg" format from:

<http://arxiv.org/ps/nlin/0005021v2>